

# Accurate mobile remote sensing of XCO<sub>2</sub> and XCH<sub>4</sub> latitudinal transects from aboard a research vessel

**F. Klappenbach<sup>1</sup>, M. Bertleff<sup>1</sup>, J. Kostinek<sup>1</sup>, F. Hase<sup>1</sup>, T. Blumenstock<sup>1</sup>,  
A. Agusti-Panareda<sup>2</sup>, M. Razinger<sup>2</sup>, and A. Butz<sup>1</sup>**

<sup>1</sup>IMK-ASF, Karlsruhe Institute of Technology (KIT), Hermann-von-Helmholtz-Platz 1, 76344  
Eggenstein-Leopoldshafen, Germany

<sup>2</sup>The European Centre for Medium-Range Weather Forecasts (ECMWF), Shinfield Park, Reading,  
RG2 9AX, UK

Correspondence to: F. Klappenbach (friedrich.klappenbach@kit.edu)

## Abstract

A portable Fourier Transform Spectrometer (FTS), model EM27/SUN, is deployed onboard the research vessel *Polarstern* to measure the column-average dry air mole fractions of carbon dioxide ( $\text{XCO}_2$ ) and methane ( $\text{XCH}_4$ ) by means of direct sunlight absorption spectrometry. We report on technical developments as well as data calibration and reduction measures required to achieve the targeted accuracy of fractions of a percent in retrieved  $\text{XCO}_2$  and  $\text{XCH}_4$  while operating the instrument under field conditions onboard the moving platform during a six week cruise through the Atlantic from Cape Town (South Africa,  $34^\circ \text{S}$ ,  $18^\circ \text{E}$ ) to Bremerhaven (Germany,  $54^\circ \text{N}$ ,  $19^\circ \text{E}$ ). We demonstrate that our solar tracker typically achieves a tracking precision of better than  $0.05^\circ$  toward the center of the sun throughout the ship cruise which facilitates accurate  $\text{XCO}_2$  and  $\text{XCH}_4$  retrievals even under harsh ambient wind conditions. We define several quality filters that screen spectra e.g. when the field-of-view is partially obstructed by ship structures or when the lines-of-sight cross the ship exhaust plume. The measurements in clean oceanic air, can be used to characterize a spurious airmass dependency. After the campaign, deployment of the spectrometer side-by-side the TCCON (Total Carbon Column Observing Network) instrument at Karlsruhe, Germany, allows for determining a calibration factor that makes the entire campaign record traceable to World Meteorological Organization (WMO) standards. Comparisons to observations of the GOSAT satellite and concentration fields modeled by the European Centre for Medium-Range Weather Forecasts (ECMWF) ~~within the project Monitoring of Atmospheric Composition and Climate — Interim Implementation (MAGG-II)~~ [Copernicus Atmosphere Monitoring Service \(CAMS\)](#) demonstrate that the observational setup is well suited to provide validation opportunities above the ocean and along interhemispheric transects.

## 1 Introduction

Carbon dioxide ( $\text{CO}_2$ ) and methane ( $\text{CH}_4$ ) are the most important anthropogenic greenhouse gases (Stocker et al., 2013). To understand their emission and uptake processes at the Earth's surface, inverse modeling approaches exploit the observed variability of the atmospheric concentration fields (e.g. Chevallier et al., 2010; Peylin et al., 2013). Estimating surface fluxes of  $\text{CO}_2$  and  $\text{CH}_4$  in particular requires accurate and spatially and temporally dense observations of the atmospheric abundances. Such observations have been delivered for decades by ground-based in-situ monitoring stations (e.g. Masarie et al., 2014) though their coverage in remote regions is sparse. Remote sensing of column-average  $\text{CO}_2$  ( $\text{XCO}_2$ ) and  $\text{CH}_4$  ( $\text{XCH}_4$ ) from satellites is an emerging technique that promises improved coverage and data density but faces challenging accuracy requirements on the order of fractions of a percent (e.g. Chevallier et al., 2007; Bergamaschi et al., 2009). Therefore,  $\text{XCO}_2$  and  $\text{XCH}_4$  soundings recorded by satellites such as Scanning Imaging Absorption Spectrometer for Atmospheric CHartography (SCIAMACHY), Greenhouse Gases Observing Satellite (GOSAT) (Burrows et al., 1995; Bovensmann et al., 1999), or the recently launched Orbiting Carbon Observatory-2 (OCO-2) require thorough validation through ground-based measurements.

To this end, the Total Carbon Column Observing Network (TCCON) has been designed, currently operating more than 20 ground-based high-resolution lab Fourier Transform Spectrometers (FTS) at stations worldwide (Wunch et al., 2011; TCCON-Wiki, 2015). These ground-based FTS collect solar absorption spectra in direct-sun view allowing for accurate knowledge of the light path through the atmosphere and thereby, avoiding one of the largest sources of error for satellite remote sensing of  $\text{XCO}_2$  and  $\text{XCH}_4$  (Rayner and O'Brien, 2001). The typical accuracy of TCCON spectrometers is reported better than 0.8 ppm (parts per million) for  $\text{XCO}_2$  and 7 ppb (parts per billion) for  $\text{XCH}_4$  (Wunch et al., 2010). The TCCON FTS operate at high spectral resolution and therefore, require stationary containers that can house the rather bulky and delicate instruments. Developments are ongoing to prove performance of smaller and more robust remote sensing instruments that can be easily

discussed in remote regions, in larger numbers, and on mobile platforms (Kobayashi et al., 2010; Krings et al., 2011; Kawasaki et al., 2012; Petri et al., 2012; Gisi et al., 2012; Frey et al., 2015).

Here, we demonstrate performance of such a small and robust spectrometer for accurate observations of XCO<sub>2</sub> and XCH<sub>4</sub> on a mobile platform. We deploy an Bruker™ EM27/SUN FTS aboard the German research vessel (RV) *Polarstern* traveling from South Africa to Germany during a 5-week cruise in March/April 2014.

The EM27/SUN FTS is a table-top, portable instrument operating at medium spectral resolution of 0.5 cm<sup>-1</sup>. Performance of the EM27/SUN FTS in stationary configuration has been proven for XCO<sub>2</sub> by Gisi et al. (2012) using measurements side-by-side the TCCON instrument at Karlsruhe, Germany. Previously, Notholt et al. (1995) and Warneke et al. (2005) have shown that RV *Polarstern* is an excellent carrier to investigate hemispheric gradients of a large variety of atmospheric constituent including the man-made greenhouse gases. Instrumentation, however, is challenged by harsh ambient conditions. In particular, the moving platform poses a challenge for direct solar absorption spectroscopy since the solar intensity has to be fed precisely into the spectrometer's entrance aperture, regardless the movements of the platform. In the view of satellite validation, shipborne measurements are particularly interesting since currently there are only a few island observatories (e.g. Geibel et al., 2010; Schneider et al., 2012) that allow for validating XCO<sub>2</sub> and XCH<sub>4</sub> derived from glint-mode satellite operations over the oceans.

Figure 1 illustrates the track of RV *Polarstern* starting out at Cape Town, South Africa (34° S, 18° E) on 5 March 2014, and entering port at Bremerhaven, Germany, (54° N, 19° E) on 14 April 2014. During the cruise the EM27/SUN spectrometer operated whenever cloud conditions permitted direct-sun view on 31 out of 40 days, in total collecting 5693-5738 spectra for which XCO<sub>2</sub> and XCH<sub>4</sub> can be derived. Beside recording solar absorption spectra, our housekeeping infrastructures monitored ambient pressure and temperature. Further, RV *Polarstern* is equipped with a meteorological station. In addition to the EM27/SUN, we operated a custom-built grating spectrometer. Design and performance of the latter will be reported in a forthcoming study.

Here, we first outline the instrument setup (Sect. 2) in particular focusing on a custom-built sun-tracker attached to the sun-viewing spectrometer. The sun-tracker must be able to **compensates** compensate both, the relatively slow motion of the solar disk across the sky and the, occasionally, fast movements of the platform. Then, we detail data reduction measures to guarantee high accuracy and consistency of the XCO<sub>2</sub> and XCH<sub>4</sub> soundings throughout the ship cruise (Sect. 3). Finally, we illustrate the usefulness of the derived greenhouse gas concentrations for validation soundings from GOSAT and for evaluating the hemispheric concentration gradients in a global model (Sect. 4). Section 5 concludes the study.

## 2 Instrumentation

The key instrumentation consists of the EM27/SUN FTS (Sect. 2.2) available for purchase at Bruker™ Optics and a custom-built solar tracker (Sect. 2.1).

### 2.1 Custom-built solar tracking system

The solar tracker is based on the “Cam-tracker” setup initially designed for stationary platforms by Gisi et al. (2011). Here, it is modified for mobile applications and its performance is demonstrated through its operation on RV *Polarstern*. The system consists of two mirrors that rotate along an azimuth and elevation axis driven by two stepper motors and it is able to point toward every point on the sky hemisphere above the instrument. A camera observes the solar image centered about the entrance aperture of the spectrometer. An image analysis software fits circles to the solar image and the aperture. The mismatch between the circle centers drives a PID (proportional-integral-differential) control unit which adjusts the mirrors to finally recenter the solar image. On stationary platforms, PID control cycles exceeding a second are acceptable given that the solar disk moves slowly across the sky. Under such conditions, Gisi et al. (2011) shows that tracking errors are typically less than 0.003° which is well below the targeted tracking accuracy of 0.05° needed to keep pointing-induced XCO<sub>2</sub> errors below 0.1 ppm.

Adapting the solar tracking system to mobile applications poses two major challenges:

- At start-up or after interruptions of the tracking operations, the solar tracker needs to find the solar disk without knowledge of the observatory's orientation. For stationary operations the attitude of the observatory is typically given at start-up (and left unchanged) and astronomical calculations provide the initial relative position of the sun.
- The PID control cycle needs to cope with the potentially fast motion of the platform in addition to the slow motion of the solar disk.

Basically, the tracking procedure can be split into two parts, that tackle the required adaptations: the coarse and the fine-tracking mode. The latter is a refinement of the concept proposed by Gisi et al. (2011). Both require additional or exchange of hardware.

The coarse-tracking mode relies on a  $185^\circ$  fish eye-lens (Lensation, BFM2320) mounted on a CMOS digital camera (VR-magic, model C-9+ PRO BW CMOS,  $1288 \times 1032$  pixel) observing the sky hemisphere above the instrument. The approximate position of the solar disk is identified as the brightest spot on the camera image. A lookup-table generated through lamp calibration in our laboratory translates image positions into azimuth and elevation angles of the tracking mirrors. The angular resolution of the coarse-tracking is approximately  $0.15^\circ \text{ pixel}^{-1}$  and strongly variable within the field of view. Thus, it is not accurate enough to perform the entire tracking process with the desired accuracy of  $0.05^\circ$ . But, the coarse-tracking ensures that the solar disc of about  $0.53^\circ$  diameter can be located within the Field-Of-View (FOV) of the fine-tracking camera, that is approximately  $10\text{--}15^\circ$ .

Once the solar image is within the FOV of the fine-tracking camera (VR-magic, model C-9+ PRO BW CMOS,  $1288 \times 1032$  pixel,  $f = 50$  mm), coarse-tracking goes idle and fine-tracking mode takes over centering the solar image on the aperture of the spectrometer through a circle fitting routine. In order to enhance the tracking velocity for a moving platform, it is essential to update the motor control parameters (position, speed or acceleration) as frequently as possible. To minimize the time lost during communication between the fine-tracking camera and the control unit (Embedded PC-System, ARK by Advantech), the

camera only transmits a region of interest of approximately  $200 \text{ pixel} \times 200 \text{ pixel}$  out of the full camera frame of  $1288 \text{ pixel} \times 1032 \text{ pixel}$  via USB. Additionally each motor connects via its own RS485 connection to the control unit to enable simultaneous send and receive to/from both motors. Based on this hardware setup, our custom-built image acquisition, processing, PID and motor control software achieves control cycle durations on the order of 20–30 ms corresponding to an update frequency of 33–50 Hz. Table 1 summarizes individual contributions.

We evaluate onboard performance of the solar tracker by examining the deviations between the center of the solar image and the targeted center of the spectrometer aperture. The deviations are logged during the entire campaign on board RV *Polarstern*. While such an assessment provides an estimate of the tracking precision, it does not allow for quantifying systematic tracking errors e.g. due to a misalignment of the actual and the assumed center of the spectrometer aperture. A misalignment of the latter kind leads to a systematic pointing offset i.e. the solar tracker does not point exactly to the center of the sun but slightly to the limb. Fine-tracking camera and aperture are carefully aligned in the lab to avoid such systematic errors.

Figure 2 (left) shows the logarithmic occurrence count of tracking deviations in azimuth and elevation directions. The desired tracking accuracy of  $0.05^\circ$  is red encircled. 98.7 % of the entire campaign data is within this tracking error regime. The record includes all kinds of interruptions such as shadowing by the ship's infrastructure or cloudy conditions. The tracking accuracy of the entire data accounts for  $0.0076^\circ$  ( $1\sigma$ ), which means, that 68.3 % of all data points feature an accuracy of this value or better. The origin of the star-shape pattern remains unclear.

Figure 2 (right) shows the dependency of the tracking precision on the angular acceleration for an illustrative day of the ship cruise. Because the PID-parameters had been changed along the entire cruise we focus on that representative day. To simplify the evaluation just the azimuth component is analyzed. The azimuth component is physically the most inert part of the system and serves as a conservative estimate. The elevation component, however, shows very similar behavior. Generally, the larger accelerations required to

compensate ship movements, the poorer the tracking precision. The linear dependency of tracking precision on angular acceleration can be used to derive a maximum acceleration up to which our solar tracking performs within the required limits. If the angular acceleration does not exceed approximately  $6.5^\circ \text{ s}^{-2}$  the tracking precision complies with the  $0.05^\circ$  requirement.

## 2.2 Fourier Transform Spectrometer EM27/SUN

The Bruker™ EM27/SUN FTS is a table-top Fourier Transform Spectrometer of approximately 25 kg weight. It is designed in the framework of a cooperation between KIT and Bruker™ for stationary  $\text{XCO}_2$  and  $\text{XCH}_4$  measurements (Gisi et al., 2012). Here, we give a brief overview of the most important features.

The EM27/SUN is constructed as a RockSolid™ pendulum interferometer with two cube corner mirrors and a  $\text{CaF}_2$  beam splitter. The optical path difference of 1.8 cm corresponds to a spectral resolution of  $0.5 \text{ cm}^{-1}$ . A 127 mm parabolic mirror together with the 0.6 mm aperture defines an semi-FOV of 2.36 mrad. With the solar disc as light source this FOV corresponds to approximately 51.0 % of the solar diameter. The InGaAs non-cooled detector (HAMAMATSU™ G12181-010K) with a sensitive area of approximately  $0.8 \text{ mm}^2$ , has a spectral response from 5000 to  $11\,000 \text{ cm}^{-1}$ . Typical exposure times are approximately 58 s for 10 double sided interferograms, recorded in DC-mode. Differences to the prototype device used by Gisi et al. (2012) are a slightly different focal length of 127 mm instead of 101.6 mm and a detector with a spectral coverage of 5000 to  $11\,000 \text{ cm}^{-1}$  instead of 6000 to  $9000 \text{ cm}^{-1}$ . The latter adjustment was necessary to cover the spectral range of  $\text{CH}_4$  absorption. Further, a bandpass filter (Thorlabs FB1650-12, center wavenumber:  $6061 \text{ cm}^{-1}$ , FWHM:  $44.0 \text{ cm}^{-1}$ ) has been mounted in front of the internal calibration lamp in order to characterize the ghost-to-parent ratio as described in Dohe et al. (2013) or Messerschmidt et al. (2010).

Gisi et al. (2012) showed, that this instrument is highly stable against thermal influences in particular as demonstrated by observations in summer and winter in Karlsruhe. Furthermore moderate mechanical stress due to deployment and dismounting do not harm the

accuracy of the instrument. This makes the instrument in particular suitable for campaign purposes.

### 3 Data reduction and evaluation

The following section guides through the data evaluation process. Section 3.1 describes the spectral retrieval of absorber total columns from the recorded solar absorption spectra. Various quality filters (Sect. 3.2) and corrections (Sect. 3.3) guarantee that quality of the estimated  $X_{\text{CO}_2}$  and  $X_{\text{CH}_4}$  is consistently high throughout the ship cruise.

#### 3.1 Spectral retrieval

The spectral retrieval of absorber total columns uses the software package PROFFIT v.9.6 (Hase et al., 2004). In principle, PROFFIT is capable of retrieving vertical profile information from high spectral resolution measurements of the atmospheric transmittance in direct-sun view (García et al., 2012). The medium resolution of  $0.5 \text{ cm}^{-1}$  of the EM27 FTS, however, is insufficient to extract profile information from the pressure and temperature dependent absorption line shapes. Therefore, here, a configuration is chosen that retrieves a scaling parameter for the a priori absorber profiles. [In particular the number of degrees of freedom \(DOF\) is chosen to be one \(DOF=1\).](#)

The absorber total columns to be retrieved are the ones of the targeted species  $\text{CO}_2$  and  $\text{CH}_4$ , and the ones of the ancillary species molecular oxygen ( $\text{O}_2$ ) and water vapor ( $\text{H}_2\text{O}$ ). The latter is an interfering species.  $\text{O}_2$  is used to calculate the dry air mole fraction  $X_{\text{gas}}$  of the desired target gas via

$$X_{\text{gas}} = 0.209420 \cdot \frac{C_{\text{gas}}}{C_{\text{O}_2}} \quad (1)$$

where  $C_{\text{gas}}$  is the gas total column in units  $\text{molec m}^{-2}$ . Referencing the targeted gas abundance to the known  $\text{O}_2$  abundance is a common approach to cancel out instrument and retrieval related errors common to the retrievals of  $\text{O}_2$  and the target species.

The a priori profiles of CO<sub>2</sub> and CH<sub>4</sub> are taken from ~~a CarbonTracker model run (Peters et al., 2007) for the year 2008 and from a Tracer Model 4 (TM4) run (Meirink et al., 2006) for the year 2007, respectively~~ the CAMS global cyclic 1-day forecasts which is based on the ECMWF Integrated Forecasting System (IFS) as documented by (Agusti-Panareda et al., 2014) and (Massart et al., 2014). The H<sub>2</sub>O profiles are from the IFS 1-day forecasts extracted from the same model simulation as CO<sub>2</sub> and CH<sub>4</sub>. All profiles are temporally and spatially interpolated on the model grid (0.5° x 0.5° x 3 hourly) in order to avoid discontinuities. The top level of CAMS (0.1 hpa ≈ 65 km height) is being extrapolated upon ≈ 120 km height in order to fit the the evaluation layers. Meteorological parameters such as pressure and temperature vertical profiles are based on the monthly latitudinal mean profiles provided by CIRA-86<sup>1</sup> (Fleming et al., 1988) that reaches up to 120 km height in 77 levels. If available, these meteorological profiles are supplemented by the daily noon-time radiosonde measurements from aboard RV *Polarstern* reaching altitudes up to 30 km height (König-Langlo, 2014). If no radiosonde data available, the data from the global model reanalysis from the National Centers for Environmental Prediction (NCEP) (Kalnay et al., 1996) is used to supplement the initial profile up to approximately 30 km height. The NCEP-data is downloaded via the Goddard auto mailer system (Schoeberl et al., 2014). This combined profile is interpolated on a 49 layer grid from measurement height up to to 120 km.

The a priori O<sub>2</sub> ~~and profiles are generic profiles, that represent profile a priori is a generic static profile, that represents~~ a typical situation.

The calculation of atmospheric gas absorption lines are based on the High resolution TRANsmission (HITRAN) database (Rothman et al., 2009) from 2008. Whereas for CH<sub>4</sub> the unchanged line list is used, the CO<sub>2</sub> line list is modified as suggested by Lamouroux et al. (2010) to take into account line-mixing effects. The line list for O<sub>2</sub> is modified according to TCCON recommendations. Finally, the H<sub>2</sub>O line list is based on HITRAN-updates from 2009.

---

<sup>1</sup>CIRA stands for “COSPAR International Reference Atmosphere”, whereas COSPAR stands for “Committee on SPACE Research”.

Table 2 gives an overview of the most important retrieval parameters among the various spectral windows.

The Instrumental Line Shape (ILS) of the instrument is determined analyzing water vapor absorption lines along a light path through ambient air in our laboratory. A 50 W light bulb is collimated and positioned at  $\sim 4.0$  m distance to the spectrometer. A data logger (MRC, MHB-382SD) provides temperature and pressure readings to calculate the appropriate absorption line shapes. Parameters defining the ILS are retrieved together with the ambient  $\text{H}_2\text{O}$  abundance from absorption spectra in the spectral range at  $7000\text{--}7400\text{ cm}^{-1}$  using the LINEFIT software package version 14 (Hase et al., 1999). ILS retrieval parameters are 0.99594 for the modulation efficiency and  $2.83 \times 10^{-3}$  for the phase error in the post campaign retrieval. As long as no instrumental changes (e.g. accidental or intentional changes in the optical alignment) are undertaken, the inferred ILS parameters have been shown to be constant over month-long timescales (Gisi et al., 2012; Frey et al., 2015). ~~During the RV *Polarstern* cruise, the instrument housing had to be removed which appears to have caused a slight change of the optical alignment. To monitor and mitigate changes in the ILS, we conduct a preprocessing step which retrieves the ILS parameters from absorption lines throughout the ship cruise. Details are given in Sect. 3.3.~~

The preprocessing was performed with the python routine “Calpy\_mobile” programme developed at KIT. This routine requests and downloads the meteorological profile data at the Goddard automailer system and generates the input profiles with the radiosonde data. Additionally it performs the DC-correction (Keppel-Aleks et al., 2007a) (see Sect. 3.3) on the interferogram, the fourier transformation and finally exports it into a binary input format for PROFFIT.

### 3.2 Quality filters

The spectrometer was operated semi-automatically from morning to afternoon on deck of the RV *Polarstern* whenever outside weather conditions were not too harsh. Therefore, spectra were recorded also under unfavorable conditions e.g. when the sun was partially obscured by ship structures or when lines-of-sight crossed the exhaust plume (EP) of the

ship. To exclude such measurements from the scientific data set, we apply three quality filters: The DC-filter screens strong intensity fluctuations. The O<sub>2</sub>-filter gives an estimate on the retrieval quality with the ground pressure as reference. Finally the EP-filter (Exhaust Plume) removes measurements, where the instrument's line of sight passed the ships exhaust plume.

The DC-filter is designed to sort out intensity fluctuations during the measurement. These fluctuations can for example be introduced by variable cirrus clouds or by the ship's structures obscuring the line-of-sight. We operate the EM27/SUN FTS in the DC-mode i.e. the spectrometer records the full interferogram including its smoothly varying DC part. Strong fluctuations in the DC part are indicative for varying source brightness. Affected measurements can be corrected with the low pass filtered interferogram  $I_{lp}$  (Keppel-Aleks et al., 2007b). The implementation of the low pass is a running mean on the interferogram over 61 sampling points with 5 iterations.

However, this DC-correction ~~removes not~~ does not remove the entire DC-effect, and especially strong variations still appear to influence the retrieval result. Based on the DC-correction, a filter criterion DC can be defined to sort out affected measurements:

$$DC = \frac{|I_{lp}|_{\max} - |I_{lp}|_{\min}}{|I_{lp}|_{\max}}. \quad (2)$$

The higher the value of the DC criterion, the stronger the effect on the retrieved trace gas. Effects of the DC filter are examined in Figs. 3 and 4 and discussed together with the next filter. Here, we choose a filter threshold  $DC < 0.05$  that discards ~~21.223.2~~ 21.223.2% of the recorded spectra.

The O<sub>2</sub>-filter is based on the comparison between surface pressure calculated from the retrieved O<sub>2</sub> column and the in-situ measured surface pressure (König-Langlo, 2014) as suggested by Wunch et al. (2011). Deviations indicate a false measurement since the O<sub>2</sub> concentration in the atmosphere can be assumed constant. Taking into account a scaling factor of ~~0.9717~~ 0.9705 for calibrating the spectroscopically retrieved surface pressure  $p_{retr}$

to the in-situ measurements  $p_{\text{in-situ}}$  (Wunch et al., 2011), the ratio

$$R_{\text{psf}} = \frac{0.9717 \times p_{\text{retr}}}{p_{\text{in-situ}}} \frac{0.9705 \times p_{\text{O}_2} + p_{\text{H}_2\text{O}}}{p_{\text{in-situ}}} \quad (3)$$

scatters around unity. Here, we screen spectra whenever  $R_{\text{psf}}$  deviates by more than 0.3 % from unity removing ~~7.26.3~~ % of the DC-filtered spectra. To determine the filter thresholds for both the DC- and  $\text{O}_2$ -filter, we define a quality criterion  $Q$  for the retrieved  $\text{XCO}_2$ : we select a subset of representative days from 22 to 25 March. First, we remove diurnal variations from the record by fitting a 3rd order polynomial for each day and subtracting the polynomial from the retrieved  $\text{XCO}_2$ . The standard deviation of the residual  $\text{XCO}_2$  timeseries defines our quality criterion  $Q$  in units of ppm.

Figure 3 illustrates how the DC-filter and the  $\text{O}_2$ -filter affects the quality criterion  $Q_{\text{XCO}_2}$ . In general the stricter the filter thresholds the better the precision but the fewer data passing the quality filters. Figure 4 shows the  $\text{XCO}_2$  measurements for these four representative days and the effect of the DC- and  $\text{O}_2$  filters with the selected thresholds. The overlap of the two filters is very little, showing that they filter for independent effects.

Under the assumption, that the 3rd order polynomial removes all geophysical variability due to local surface fluxes and advective transport, this quality criterion provides a precision estimate for the EM27/SUN amounting to  ~~$Q_{\text{XCO}_2} = 0.13$~~   $Q_{\text{XCO}_2} = 0.11$  ppm for  $\text{XCO}_2$ . Following an ~~analogue~~ analogous procedure for  $\text{XCH}_4$  yields  ~~$Q_{\text{XCH}_4} = 0.62 \times 10^{-4}$~~   $Q_{\text{XCH}_4} = 0.61$  ppb.

The third filter is the exhaust-plume filter (EP-filter). The ship's ~~smoke pipe~~ funnel is located at a few ten meters distance to the spectrometer setup and rises to approximately 12 m above deck. If the line-of-sight passes through the exhaust plume, enhancements in the observed  $\text{XCO}_2$  are to be expected. In order to screen such observations, we calculate the enhancement pattern in the  $\text{XCO}_2$  time series from our line-of-sight (los), the prevailing wind conditions and the ship's exhaust.

A estimated exhaust flux  $E_s$  feeds a simple plume model that calculates the  $\text{XCO}_2$  enhancement  $E_{\text{los}}$  taking into account the relative wind speed and direction between the ship-

based spectrometer and the plume. We rely on the plume diffusion model used by Bovensmann et al. (2010). Defining the  $x$  coordinate as downwind direction and the  $y$  coordinate as the crosswind direction, the enhancement  $E_{\text{los}}$  along the line-of-sight can be calculated via

$$E_{\text{los}} = \int_{\text{los}} \frac{E_s}{v_{\text{rel}}} \frac{1}{\sqrt{2\pi} \cdot \sigma_y(x)} \cdot \exp\left(-\frac{1}{2} \frac{y^2}{\sigma_y(x)^2}\right) dx dy \quad (4)$$

where  $v_{\text{rel}}$  is the relative wind velocity between ship and plume, and the parameter  $\sigma_y(x) = 0.104 \cdot x^{0.894}$  dilutes the plume in crosswind direction ( $y$ ). Thereby, we assume a class C for the atmospheric stability (Bovensmann et al., 2010). Here the exhaust flux  $E_s := 1$  is given in arbitrary units (AU). Relative wind velocities  $v_{\text{rel}}$  and directions are taken from the records of the onboard meteorological station. The line-of-sight from instrument position up to 30 m is projected into the downwind ( $x$ ) and crosswind ( $y$ ) direction and then,  $E_{\text{los}}$  is calculated by numerically integrating Eq. (4). Figure 5 shows a day where according to the lab book the line-of-sight passed the exhaust plume as confirmed by the record of relative wind velocities and directions. Measured  $\text{O}_2$  columns and  $\text{XCH}_4$  are not affected by the ship's exhaust,  $\text{XCO}_2$ , however, is found enhanced by up to 2 ppm. Our model yields an enhancement  $E_{\text{los}}$  that is similar in temporal pattern to the observed  $\text{XCO}_2$  enhancement confirming the overall applicability of our approach.

The EP-filter threshold is set such that whenever  $E_{\text{los}}$  is larger than 0.001 the spectrum is flagged contaminated. ~~11.6~~11.1 % of the spectra are discarded by the EP-filter. Additionally, 2.8 % of the spectra are rejected due to contamination by the exhaust plume after inspection by eye.

In total, the three filters (DC,  $\text{O}_2$  and EP) described above screen about ~~37.5~~38.2 % of the recorded spectra.

### 3.3 Corrections

~~Three~~Two major corrections are found necessary to make the  $\text{XCO}_2$  and  $\text{XCH}_4$  records consistently accurate along the ship cruise: a ~~change of the instrumental line shape (ILS)~~

~~of the FTS has to be taken into account, a spurious dependency of the retrieved target gas abundances on solar zenith angle needs to be corrected, and an overall calibration factor needs to be found to make the spectroscopic measurements consistent with the WMO (World Meteorological Organization) calibration scale.~~

~~It was required to open the EM27/SUN FTS instrument housing on 18 March 2014: The instrument has the option to toggle the incoming light beam between an internal calibration lamp and the external measurement input. This switch is implemented by a movable, flat mirror, located inside the instrument's housing. The mechanics of this mirror was jammed by the additional optical filter (see Sect. 2.2), that we mounted in front of the calibration lamp. We opened the housing and removed the blocking features successfully. However, it turns out that this caused a slight change of the ILS. To cope with this change, we perform an initial test retrieval in the window with the ILS modulation efficiency as a free parameter as described in Sect. 3.1. Figure ?? shows a change of about 1 of the retrieved ILS parameter on the day when the instrument housing was opened. Here, we use the ILS determined by post-campaign measurements for spectra collected after 18 March 2014. For data collected before opening the instrument housing, we use the same post-campaign ILS but modulation efficiency reduced by 1. If we process the entire campaign adopting the post-campaign ILS, the difference in is approximately 0.14 and -0.10 for -~~

A well known (e.g. Deutscher et al., 2010; Wunch et al., 2011), spurious dependency of XCO<sub>2</sub> and XCH<sub>4</sub> retrieved from TCCON measurements on slant airmass  $A$ , defined as  $A = 1/\cos(\theta)$  with solar zenith angle  $\theta$ , can be reproduced by the campaign data. The higher the airmass the lower the XCO<sub>2</sub> and the XCH<sub>4</sub> retrievals. The source of this effect remains unclear. ~~Although~~, although uncertainties of spectroscopic line broadening parameters and shortcomings of the Voigt line shape model, are likely candidates. Wunch et al. (2011) suggest an empirical correction based on a diurnal effect combined with a  $\theta$ -dependent term. Figure 6 shows that also our XCO<sub>2</sub> and XCH<sub>4</sub> retrievals clearly correlate with SZA. Given that the retrieved surface pressure derived from retrieved O<sub>2</sub> columns shows no such dependency, it must be driven by the CO<sub>2</sub> and CH<sub>4</sub> column retrievals. To correct for this

artifact, we fit a correction polynomial  $c_{\text{SZA, gas}}$  for the gases  $\text{CO}_2$  and  $\text{CH}_4$  according to

$$c_{\text{SZA, gas}}(\theta) = a \cdot |\theta|^3 + b \cdot |\theta| + c \quad (5)$$

where  $a$ ,  $b$ ,  $c$  are free fitting parameters. Thereby, the correction is by definition chosen to vanish at  $\theta = 45^\circ$  as suggested by Wunch et al. (2011) with referencing the measurement to  $\theta = \pm 45^\circ$  for forenoon and afternoon separately. The corrected  $\text{XCO}_2$  and  $\text{XCH}_4$  records are then calculated through

$$X_{\text{SZA, gas}} = \frac{X_{\text{gas}}(\theta)}{c_{\text{SZA, gas}}(\theta)}. \quad (6)$$

Figure 6 shows the retrieved correction parameters. For the extreme case of  $\theta = 80^\circ$  relative to  $\theta = 0^\circ$ , the correction amounts to  $\approx 0.60,4\%$  for  $\text{XCO}_2$  and  $\approx 0.40,3\%$  for  $\text{XCH}_4$ . A key assumption for this correction is that the measurements take place far away from localized sources and sinks of  $\text{CO}_2$  and  $\text{CH}_4$ . So, no diurnal concentration cycles are to be expected that correlate with the assumed spurious airmass dependence. Generally, this assumption appears true for our ship-borne measurements above the Atlantic. Meteorological transport can cause advection of diurnal concentration variability from the larger source/sink region. Over the course of the entire measurement campaign, we assume that such transport effects have a statistical pattern such that the airmass correction is not contaminated in a systematic way.

Finally, we calibrate the entire campaign records to the official WMO validated TCCON station at Karlsruhe, Germany ([TCCON-ka](#)). To this end, we operate our EM27/SUN side-by-side the Karlsruhe TCCON instrument during 4 consecutive days in May 2014 after the ship campaign. TCCON  $\text{XCO}_2$  and  $\text{XCH}_4$  are retrieved by the standard G-Fit v.0.4.4 software (Wunch et al., 2011). Retrievals from EM27/SUN measurements follow the approach outlined above including the quality filters described in Sect. 3.2 and the aforementioned correction terms. Hourly means  $\langle X \rangle_h$  of the  $\text{XCO}_2$  and  $\text{XCH}_4$  are calculated and used to

determine the calibration factor  $\gamma_{\text{gas}}$  according to

$$\gamma_{\text{gas}} = \left\langle \frac{\langle X_{\text{EM27}} \rangle_{\text{h}}}{\langle X_{\text{wmo}} \rangle_{\text{h}}} \right\rangle \quad (7)$$

where brackets indicate averaging over the entire dataset. The EM27/SUN measurements are then referenced to WMO via

$$X_{\text{gas,wmo}} = \frac{X_{\text{gas}}}{\gamma_{\text{gas}}}. \quad (8)$$

Figure 7 shows the post campaign reference measurements.

We find calibration factors  $\gamma_{\text{XCO}_2} = (0.99195 \pm 0.00051)$  and  $\gamma_{\text{XCH}_4} = (0.98211 \pm 0.00146)$  where the error estimate refers to the standard deviation among the calibration data set. Note that the calibration factor for  $\text{O}_2$  (see Sect. 3.2) in the order of  $\approx 2.8\%$  ( $\approx 0.972$ ) is still present in the un-referenced data and is included into the calibration factor  $\gamma_{\text{gas}}$ . Note further, that this calibration is already for the reprocessed TCCON-ka data set. This improvement was found to be necessary because the station Karlsruhe differs in the optical setup from other TCCON stations (M.Kiel, personal communication, in preparation 2015). The difference scales  $\gamma_{\text{XCO}_2,\text{old}}/\gamma_{\text{XCO}_2,\text{new}} = 1.00219487$  and  $\text{XCH}_4$  by  $1.00103463$ .

#### 4 XCO<sub>2</sub> and XCH<sub>4</sub> over the Atlantic

Figure 8 shows the final XCO<sub>2</sub> and XCH<sub>4</sub> records measured above the Atlantic in March/April 2014 from aboard RV *Polarstern*. All corrections (see Sect. 3.3) and quality filters (see Sect. 3.2) are applied. In order to motivate the usefulness of such ship deployments for satellite and model validation, Fig. 8 additionally shows satellite soundings from the Greenhouse Gas Observing Satellite (GOSAT) and XCO<sub>2</sub> and XCH<sub>4</sub>

modeled by the ~~MAGC-II (Monitoring Atmospheric Composition and Climate — Interim Implementation)~~ CAMS (Copernicus Atmosphere Monitoring Service) data assimilation and forecasting system (Agustí-Panareda et al., 2014; Massart et al., 2014). Satellite soundings correlated to RV *Polarstern* records with an 5° latitudinal/longitudinal radius in addition with a 4 h temporal coincidence radius (see Fig. 1). Model data is being temporally and spatially interpolated to the RV *Polarstern* measurements to avoid discontinuities.

The lower panel shows the differences of the various greenhouse gas products to the campaign record. Here averages of all EM27/SUN soundings within the coincidence criteria is subtracted from the individual satellite soundings.

For GOSAT, we discuss three different GOSAT retrieval methods, the RemoTeC-Full-Physics (FP) and RemoTeC-Proxy (Butz et al., 2011; Guerlet et al., 2013; Schepers et al., 2012) retrieval as well as the Atmospheric CO<sub>2</sub> Observations from Space (ACOS) approach (O'Dell et al., 2012; Crisp et al., 2012). Even though the in-orbit operations of GOSAT have been adapted to maximize the number of ocean-glint soundings during the campaign period, the number of coincident and quality-assured retrievals amounts to a few ~~ten~~ tens of samples, largely varying among the retrieval approaches. The main difference between the RemoTeC-FP and the RemoTeC-Proxy algorithm is the way the lightpath through the atmosphere is estimated. While RemoTeC-FP retrieves aerosol parameters simultaneously with XCO<sub>2</sub> and XCH<sub>4</sub> and takes multiple scattering effects into account, the RemoTeC-Proxy approach is restricted to XCH<sub>4</sub> only and uses the retrieved CO<sub>2</sub> column together with CarbonTracker-modeled CO<sub>2</sub> as a lightpath proxy. ACOS is, as well as RemoTeC-FP, a full-physics approach i.e. simultaneously retrieving XCO<sub>2</sub> and atmospheric scattering properties. Differences between RemoTeC-FP and ACOS relate to details how aerosol and cloud scattering parameters are implemented and how the inverse problem is solved. Most importantly here, ACOS delivers many more data than RemoTeC-FP for ocean-glint soundings since RemoTeC-FP resorts to a conservative cloud and aerosol filtering scheme using the “upper edge” method (Butz et al., 2013). ACOS does not deliver XCH<sub>4</sub>. For the comparison with all the GOSAT products the smoothing effect of the averaging kernel matrix

is neglected. Compared to systematic errors introduced by temporal and spatial distance we consider these effects as negligible.

The ~~MAGG-II CAMS~~ provides global operational analysis and forecast of CO<sub>2</sub> and CH<sub>4</sub> in near real time. Here we have used a forecast without any data assimilation with a horizontal resolution of around 80 km and 60 vertical levels from surface to 0.1 hPa. The atmospheric CO<sub>2</sub> and CH<sub>4</sub> concentration-mixing ratio fields modeled by ~~MAGG-II CAMS~~ rely on the ~~Integrated Forecasting System (IFS) model operated by ECMWF~~ ECMWF IFS model<sup>2</sup>. The IFS has a simple carbon module (Boussetta et al., 2013) to model the CO<sub>2</sub> uptake and release from vegetation. The CO<sub>2</sub> biogenic fluxes from vegetation are adjusted to correct for large-scale biases by using a climatology of optimized CO<sub>2</sub> fluxes (Agusti-Panareda et al., 2015, ECMWF Tech Memo 2015). The CH<sub>4</sub> fluxes and other CO<sub>2</sub> fluxes are prescribed by inventories and seasonally varying climatologies, including the chemical sinks for CH<sub>4</sub> in the troposphere and stratosphere. A more detailed description of the CO<sub>2</sub> and CH<sub>4</sub> forecast configuration can be found in Agustí-Panareda et al. (2014) for CO<sub>2</sub> and in Massart et al. (2014) for CH<sub>4</sub>. The plotted data stems from the ~~“gb5b” model experiment where no assimilation-model simulation where the meteorology is re-initialized daily using ECMWF meteorological analyses but~~ CO<sub>2</sub> and CH<sub>4</sub> are free running, i.e. no assimilation of CO<sub>2</sub> and CH<sub>4</sub> observations is performed.

The EM27/SUN XCO<sub>2</sub> measurements from aboard RV *Polarstern*, Fig. 8 (left), show a North–South (N–S) gradient of up to 56.8 ppm between  $\sim 45^\circ$  N and  $\sim 30^\circ$  S at the end of the Northern Hemisphere dormant season. This is largely expected from previous assessments (e.g. Denning et al., 1995). Beside the N–S gradient, diurnal and day-to-day variations on the order of 1 ppm are found most likely originating from transport of far-away source/sink signals. Note that the exhaust of RV *Polarstern* itself is excluded from the data via the EP-filter (see Sect. 3.2).

For XCH<sub>4</sub>, Fig. 8 (right), the EM27/SUN soundings find a N–S gradient of roughly 0.06 ppm between  $\sim 45^\circ$  N and  $\sim 30^\circ$  S. Diurnal and day-to-day variability on the order of 0.01 to 0.02 ppm can be observed around  $30^\circ$  S  $35^\circ$  N. Tentatively, latitudinal variability in

---

<sup>2</sup>[software.ecmwf.int/wiki/display/IFS/Official+IFS+Documentation](https://software.ecmwf.int/wiki/display/IFS/Official+IFS+Documentation)

XCH<sub>4</sub> and XCO<sub>2</sub> follows similar patterns. For example, one might speculate whether XCO<sub>2</sub> and XCH<sub>4</sub> increasing towards the Northern tropics (~ 10° N) are related to emissions of both gases from biomass burning. Though, the inner tropics lack data to confirm that hypothesis.

Both GOSAT XCO<sub>2</sub> retrievals, RemoTeC-FP and ACOS, generally match the EM27/SUN observations within 2 ppm. Due to sparse data coverage, RemoTeC-FP does not allow for assessing the N–S gradient. The ACOS retrievals tentatively show a weaker N–S gradient due to XCO<sub>2</sub> land-nadir soundings North of 23° being somewhat lower than the ship records. Scatter of the data, however, hinders robust conclusions.

The GOSAT RemoTeC-FP and RemoTeC-Proxy XCH<sub>4</sub> retrievals, both agree with the ship-borne records to mostly within 0.02 ppm. As for XCO<sub>2</sub>, the yield from RemoTeC-FP is too low to infer robust conclusions but overall RemoTeC-FP delivers XCH<sub>4</sub> offset by 0.01 to 0.02 ppm compared to RemoTeC-Proxy retrievals. The latter fit the validation data particularly well for the tropical ocean-glint soundings. The land-nadir soundings North of 23° N show greater differences of 0.03 to 0.04 ppm i.e. both, RemoTeC-Proxy XCH<sub>4</sub> and ACOS XCO<sub>2</sub>, reveal larger differences for the Northern mid-latitude land-nadir observations than for the low-latitude ocean-glint soundings. Given that both algorithms and both species are affected, the most likely explanation is that our coincidence criterion is too loose to assume homogeneous concentration fields in the mid-latitudes.

~~The XCO<sub>2</sub> modeled by MAGG-II shows modeled by CAMS shows an overall~~ excellent agreement to our ship-borne records. In the northern extratropics an offset of 1 to 2 ppm is consistent with an independent evaluation done by Agusti-Panareda et al. (2015, ECMWF Tech. Memo) using TCCON data at several sites in the Northern extratropics. Even small variations, typically Hemisphere extratropics. This model bias is linked to errors in the modelled CO<sub>2</sub> fluxes which will be addressed by the CO<sub>2</sub> flux adjustment scheme under development in the CAMS forecasting system. Despite this mode bias, the small variations introduced by transport processes, can be resolved by both, model and measurement. North of the tropics model-measurement agreement is better than 1. Differences are particularly model and measurements. Differences are larger in the trop-

ics where the model overestimates XCO<sub>2</sub>. ~~The~~ It is clear that the model is not able to represent accurately the CO<sub>2</sub> emissions from West Africa characterized by widespread biomass burning. Due to persistent cloud cover the ship records lack data in the inner tropics due to persistent cloud cover. Largest discrepancies up to 2.0 that hinders further investigation of this source related error. Smaller discrepancies of less than 1 ppm are found in the Southern Hemisphere showing a persistent underestimation. For our demonstrator study, we neglect effects due to background air. The smoothing effects introduced by the averaging kernel of the measurements. Such effects might be of relevance for the level of agreement found for in the Northern extratropics but are assumed negligible for the larger differences in the Southern Hemisphere or the inner tropics matrix are directly taken into account due to the use of the model a priories for the spectral retrieval. These effects are larger in the northern extratropics and tropics, but are found to be negligible in the southern extratropics. For XCH<sub>4</sub>, model-measurement deviations are below ~~0.020.2~~ ppm for most of the cases. ~~There is no systematic underestimation in the Southern Hemisphere as it is the case for.~~

~~However, both models increasingly overestimate the and~~ The discrepancies are also larger in the northern hemisphere where XCH<sub>4</sub> towards the inner tropical convergence zone (ITGZ). Here, the relative deviation is larger for fluxes are strongest, but the relative differences are much smaller than for XCO<sub>2</sub>, that might point to deficiencies of the assumed surface fluxes and/or the efficiency of the chemical sink for in tropical regions.

Overall, the deployment of the EM27/SUN spectrometer on RV *Polarstern* demonstrates that the inferred latitudinal transects of XCO<sub>2</sub> and XCH<sub>4</sub> are of adequate quality to validate soundings from satellites such as GOSAT and to evaluate modeled concentration fields such as provided by the MAGG-II-CAMS model. The observations collected during our ~ 5 week campaign are too sparse too allow for a statistically robust ensemble of coincidences with GOSAT but demonstrate the potential for providing satellite validation over the oceans where other validation opportunities are sparse. Already a few ship cruises, similar to the one discussed here, conducted per year would make a great asset to for XCO<sub>2</sub> and XCH<sub>4</sub> remote sensing from satellites in particular for satellites such as OCO-2 providing

much denser data coverage than GOSAT. Despite the snapshot-like nature of our observations, the comparison of the ship records to the MAGG-II CAMS model hints at deficiencies in the inter-hemispheric transport of the model and potentially, erroneous tropical surface fluxes for ~~-. Thereby, simultaneously model errors in the~~ CO<sub>2</sub> and CH<sub>4</sub> surface fluxes and model deficiencies in the representation of the chemical sink for XCH<sub>4</sub> in tropical regions. Simultaneously comparing measured and modeled XCO<sub>2</sub> and XCH<sub>4</sub> delivers additional confidence in the conclusions since transport related errors are correlated among the two species ~~-, thus helping in the model flux/transport error source attribution.~~

## 5 Conclusions

The portable EM27/SUN FTS has been successfully used to record direct sunlight spectra on board the German research vessel “Polarstern”. The solar tracking device could be has been adapted in hard- and software such that direct-sun absorption spectra could be have been recorded regardless of the ship’s movements achieving a tracking precision better than the required  $0.05^\circ$  for 98.7 % of the onboard measurements. This implies that our tracking system can handle angular accelerations up to  $6.5^\circ \text{ s}^{-2}$ . To guarantee adequate accuracy of the retrieved XCO<sub>2</sub> and XCH<sub>4</sub> abundances, we define several quality filters and correction steps. The data are filtered for intensity fluctuations during recording of the interferogram (DC-filter), spurious variations in the retrieved O<sub>2</sub> reference (O<sub>2</sub>-filter), and XCO<sub>2</sub> retrievals contaminated by the ship’s local exhaust plume (EP-filter). After quality filtering, we correct for a slight change in the ILS during the campaign, a spurious SZA dependency of the retrieved concentration records, and an overall scaling factor with respect to the WMO calibration scale. Thus, the final XCO<sub>2</sub> and XCH<sub>4</sub> concentrations are traceable to WMO standards and show an overall precision of 0.130.11 ppm for XCO<sub>2</sub> and 6.2·10<sup>-4</sup> ppm 0.59 ppb for XCH<sub>4</sub>, respectively, as estimated from the scatter of retrieved concentrations after subtracting a polynomial background.

The campaign record of XCO<sub>2</sub> and XCH<sub>4</sub> shows the expected North to South gradient overlaid by regional meteorological transport effects. The quality of our ship-based

records allows for comparisons to XCO<sub>2</sub> and XCH<sub>4</sub> retrieved from GOSAT or modeled concentration fields. Although the number of satellite coincidences is low, both the ACOS/GOSAT XCO<sub>2</sub> and RemoTeC-proxy/GOSAT XCH<sub>4</sub> tend to underestimate the inter-hemispheric gradient due to low retrieved concentrations in the Northern extra-tropics. The comparison between the [MAGG-II-CAMS](#) model and the ship records shows excellent agreement for XCH<sub>4</sub> and a systematic ~~low-biased-high bias~~ for XCO<sub>2</sub> in the ~~Southern Hemisphere~~. [Northern Hemisphere associated with CO<sub>2</sub> surface fluxes and documented by Agusti-Panareda et al \(Deliverable, Tech Memo\)](#). These comparisons recommend our setup, based on the EM27/SUN FTS and a fast solar tracker, to be used for validating models and satellites e.g. through future deployments on moving platforms such as research vessels, other ships, or land-based vehicles.

The data collected during the RV *Polarstern* cruise is ~~public-publically~~ available on the PANGEA archive (PANGEA, 2014) [as supplement to this document or upon request](#).

*Acknowledgements.* Friedrich Klappenbach, Marco Bertleff, Julian Kostinek, and André Butz are supported by the Emmy-Noether program of the Deutsche Forschungsgemeinschaft (DFG) through grant BU2599/1-1 (RemoteC). We gratefully thank the crew of the RV *Polarstern* for their forthcoming and expert support. We thank Alfred Wegener Institute (AWI), Helmholtz Centre for Polar and Marine Research, for operating RV *Polarstern* and granting access to its infrastructures. We thank Otto Hasekamp and the RemoTeC team at the Netherlands Institute for Space Research (SRON) for co-developing the RemoTeC algorithm and providing RemoTeC/GOSAT retrievals. We thank Christopher O'Dell and the ACOS team at Colorado State University (CSU) and the NASA Jet Propulsion Laboratory for providing ACOS GOSAT retrievals. We thank Matthäus Kiel and Matthias Frey for suggesting the DC-Quality criteria. Thanks again to Matthäus Kiel for providing the initial version of “Calpy”.

~~The article-processing-charges for this open-access-publication were covered by a Research Centre of the Helmholtz Association.~~ [We acknowledge support by Deutsche Forschungsgemeinschaft and Open Access Publishing Fund of Karlsruhe Institute of Technology.](#)

## Appendix A

Remote sensing instruments are usually not uniformly sensitive to all layers in the atmosphere. The averaging kernel matrix weights the contribution of individual layers to the final retrieved column. The averaging kernel matrix depends on the ILS, solar zenith angle and other parameters. In order to compare the retrieval with other products, one has to include the averaging kernel matrix in the comparison as suggested by (Rodgers et al., 2003) and can be written as:

$$c_i = \mathbf{h}^T \mathbf{x}_i = \mathbf{h}^T \mathbf{A} \mathbf{x}_{true} + \mathbf{h}^T (\mathbf{I} - \mathbf{A}) \mathbf{x}_{apr} + \epsilon_i \quad (\text{A1})$$

Here the retrieved total column  $c_i$  from the instrument  $i$  is being calculated using the total column operator  $\mathbf{h}$  and the averaging kernel matrix  $\mathbf{A}$  on the state vector  $\mathbf{x}_i$ .  $\mathbf{x}_{true}$  is the true, usually unknown value,  $\epsilon_i$  any kind of errors and  $\mathbf{I}$  represents the unity matrix. A comparison to a high resolution profile (e.g. aircraft profile or model) can be calculated as assuming the state vector  $\mathbf{x}_{true}$  being the high resolution profile. In case of  $\mathbf{x}_{true} = \mathbf{x}_{apr}$  the smoothing effect of the averaging kernel cancels out and both profiles can be compared directly just applying the total column operator.

Applying the total column operator  $\mathbf{h}$  on the averaging kernel matrix  $\mathbf{A}$  one gets the total column sensitivity. This can be pictured as the retrieval response to a delta function perturbation in a distinct retrieval layer. Figure 9 shows the retrieval total column sensitivity for the target species  $\text{CO}_2$  and  $\text{CH}_4$  in dependence on layer pressure (height) and solar zenith angle. Deviations from the ideal value of one can only be found in very high layers or shallow solar zenith angles.

## References

Agustí-Panareda, A., Massart, S., Chevallier, F., Boussetta, S., Balsamo, G., Beljaars, A., Ciais, P., Deutscher, N. M., Engelen, R., Jones, L., Kivi, R., Paris, J.-D., Peuch, V.-H., Sherlock, V., Vermeulen, A. T., Wennberg, P. O., and Wunch, D.: Forecasting global atmospheric  $\text{CO}_2$ , *Atmos. Chem. Phys.*, 14, 11959–11983, doi:10.5194/acp-14-11959-2014, 2014.

- Bergamaschi, P., Frankenberg, C., Meirink, J. F., Krol, M., Villani, M. G., Houweling, S., Dentener, F., Dlugokencky, E. J., Miller, J. B., Gatti, L. V., Engel, A., and Levin, I.: Inverse modeling of global and regional CH<sub>4</sub> emissions using SCIAMACHY satellite retrievals, *J. Geophys. Res.-Atmos.*, 114, D22301, doi:10.1029/2009JD012287, 2009.
- Boussetta, S., Balsamo, G., Beljaars, A., Agusti-Panareda, A., Calvet, J.-C., Jacobs, C., van den Hurk, B., Viterbo, P., Lafont, S., Dutra, E., Jarlan, L., Balzarolo, M., Papale, D., and van der Werf, G.: Natural carbon dioxide exchanges in the ECMWF integrated forecasting system: implementation and offline validation, *J. Geophys. Res.-Atmos.*, 118, 1–24, doi:10.1002/jgrd.50488, 2013.
- Bovensmann, H., Burrows, J., Buchwitz, M., Frerick, J., Noël, S., Rozanov, V., Chance, K., and Goede, A.: SCIAMACHY: mission objectives and measurement modes, *J. Atmos. Sci.*, 56, 127–150, 1999.
- Bovensmann, H., Buchwitz, M., Burrows, J. P., Reuter, M., Krings, T., Gerilowski, K., Schneising, O., Heymann, J., Tretner, A., and Erzinger, J.: A remote sensing technique for global monitoring of power plant CO<sub>2</sub> emissions from space and related applications, *Atmos. Meas. Tech.*, 3, 781–811, doi:10.5194/amt-3-781-2010, 2010.
- Burrows, J., Hölzle, E., Goede, A., Visser, H., and Fricke, W.: SCIAMACHY scanning imaging absorption spectrometer for atmospheric cartography, *earth Observation, Acta Astronaut.*, 35, 445–451, doi:10.1016/0094-5765(94)00278-T, 1995.
- Butz, A., Guerlet, S., Hasekamp, O., Schepers, D., Galli, A., Aben, I., Frankenberg, C., Hartmann, J.-M., Tran, H., Kuze, A., Keppel-Aleks, G., Toon, G., Wunch, D., Wennberg, P., Deutscher, N., Griffith, D., Macatangay, R., Messerschmidt, J., Notholt, J., and Warneke, T.: Toward accurate CO<sub>2</sub> and CH<sub>4</sub> observations from GOSAT, *Geophys. Res. Lett.*, 38, L14812, doi:10.1029/2011GL047888, 2011.
- Butz, A., Guerlet, S., Hasekamp, O. P., Kuze, A., and Suto, H.: Using ocean-glint scattered sunlight as a diagnostic tool for satellite remote sensing of greenhouse gases, *Atmos. Meas. Tech.*, 6, 2509–2520, doi:10.5194/amt-6-2509-2013, 2013.
- Chevallier, F., Bréon, F.-M., and Rayner, P. J.: Contribution of the Orbiting Carbon Observatory to the estimation of CO<sub>2</sub> sources and sinks: theoretical study in a variational data assimilation framework, *J. Geophys. Res.-Atmos.*, 112, D09307, doi:10.1029/2006JD007375, d09307, 2007.
- Chevallier, F., Ciais, P., Conway, T. J., Aalto, T., Anderson, B. E., Bousquet, P., Brunke, E. G., Ciattaglia, L., Esaki, Y., Fröhlich, M., Gomez, A., Gomez-Pelaez, A. J., Haszpra, L., Krummel, P. B., Langenfelds, R. L., Leuenberger, M., Machida, T., Maignan, F., Matsueda, H.,

- Morguí, J. A., Mukai, H., Nakazawa, T., Peylin, P., Ramonet, M., Rivier, L., Sawa, Y., Schmidt, M., Steele, L. P., Vay, S. A., Vermeulen, A. T., Wofsy, S., and Worthy, D.: CO<sub>2</sub> surface fluxes at grid point scale estimated from a global 21 year reanalysis of atmospheric measurements, *J. Geophys. Res.-Atmos.*, 115, D21307, doi:10.1029/2010JD013887, 2010.
- Crisp, D., Fisher, B. M., O'Dell, C., Frankenberg, C., Basilio, R., Bösch, H., Brown, L. R., Castano, R., Connor, B., Deutscher, N. M., Eldering, A., Griffith, D., Gunson, M., Kuze, A., Mandrake, L., McDuffie, J., Messerschmidt, J., Miller, C. E., Morino, I., Natraj, V., Notholt, J., O'Brien, D. M., Oya-fuso, F., Polonsky, I., Robinson, J., Salawitch, R., Sherlock, V., Smyth, M., Suto, H., Taylor, T. E., Thompson, D. R., Wennberg, P. O., Wunch, D., and Yung, Y. L.: The ACOS CO<sub>2</sub> retrieval algorithm – Part II: Global X<sub>CO<sub>2</sub></sub> data characterization, *Atmos. Meas. Tech.*, 5, 687–707, doi:10.5194/amt-5-687-2012, 2012.
- Denning, A. S., Fung, I. Y., and Randall, D.: Latitudinal gradient of atmospheric CO<sub>2</sub> due to seasonal exchange with land biota, *Nature*, 376, 240–243, 1995.
- Deutscher, N. M., Griffith, D. W. T., Bryant, G. W., Wennberg, P. O., Toon, G. C., Washenfelder, R. A., Keppel-Aleks, G., Wunch, D., Yavin, Y., Allen, N. T., Blavier, J.-F., Jiménez, R., Daube, B. C., Bright, A. V., Matross, D. M., Wofsy, S. C., and Park, S.: Total column CO<sub>2</sub> measurements at Darwin, Australia – site description and calibration against in situ aircraft profiles, *Atmos. Meas. Tech.*, 3, 947–958, doi:10.5194/amt-3-947-2010, 2010.
- Dohe, S., Sherlock, V., Hase, F., Gisi, M., Robinson, J., Sepúlveda, E., Schneider, M., and Blumenstock, T.: A method to correct sampling ghosts in historic near-infrared Fourier transform spectrometer (FTS) measurements, *Atmos. Meas. Tech.*, 6, 1981–1992, doi:10.5194/amt-6-1981-2013, 2013.
- Fleming, E. L., Chandra, S., Schoeberl, M. R., and Barnett, J. J.: Monthly mean global climatology of temperature, wind, geopotential height, and pressure for 0–120 km, *Advances in Space Research*, 10, 3–12, doi:10.1016/0273-1177(90)90230-W, 1988.
- Frey, M., Hase, F., Blumenstock, T., Groß, J., Kiel, M., Mengistu Tsidu, G., Schäfer, K., Sha, M. Kumar, and Orphal, J.: Use of portable FTIR spectrometers for detecting greenhouse gas emissions of the megacity Berlin – Part 1: Instrumental line shape characterisation and calibration of a quintuple of spectrometers, *Atmos. Meas. Tech. Discuss.*, 8, 2735–2766, doi:10.5194/amtd-8-2735-2015, 2015.
- García, O. E., Schneider, M., Redondas, A., González, Y., Hase, F., Blumenstock, T., and Sepúlveda, E.: Investigating the long-term evolution of subtropical ozone profiles applying ground-

- based FTIR spectrometry, *Atmos. Meas. Tech.*, 5, 2917–2931, doi:10.5194/amt-5-2917-2012, 2012.
- Geibel, M. C., Gerbig, C., and Feist, D. G.: A new fully automated FTIR system for total column measurements of greenhouse gases, *Atmos. Meas. Tech.*, 3, 1363–1375, doi:10.5194/amt-3-1363-2010, 2010.
- Gisi, M., Hase, F., Dohe, S., and Blumenstock, T.: Camtracker: a new camera controlled high precision solar tracker system for FTIR-spectrometers, *Atmos. Meas. Tech.*, 4, 47–54, doi:10.5194/amt-4-47-2011, 2011.
- Gisi, M., Hase, F., Dohe, S., Blumenstock, T., Simon, A., and Keens, A.: XCO<sub>2</sub>-measurements with a tabletop FTS using solar absorption spectroscopy, *Atmos. Meas. Tech.*, 5, 2969–2980, doi:10.5194/amt-5-2969-2012, 2012.
- Guerlet, S., Butz, A., Schepers, D., Basu, S., Hasekamp, O. P., Kuze, A., Yokota, T., Blavier, J.-F., Deutscher, N. M., Griffith, D. W., Hase, F., Kyro, E., Morino, I., Sherlock, V., Sussmann, R., Galli, A., and Aben, I.: Impact of aerosol and thin cirrus on retrieving and validating XCO<sub>2</sub> from GOSAT shortwave infrared measurements, *J. Geophys. Res.-Atmos.*, 118, 4887–4905, doi:10.1002/jgrd.50332, 2013.
- Hase, F., Blumenstock, T., and Paton-Walsh, C.: Analysis of the instrumental line shape of high-resolution Fourier transform IR spectrometers with gas cell measurements and new retrieval software, *Appl. Optics*, 38, 3417–3422, doi:10.1364/AO.38.003417, 1999.
- Hase, F., Hannigan, J., Coffey, M., Goldman, A., Höpfner, M., Jones, N., Rinsland, C., and Wood, S.: Intercomparison of retrieval codes used for the analysis of high-resolution, ground-based FTIR measurements, *J. Quant. Spectrosc. Ra.*, 87, 25–52, doi:10.1016/j.jqsrt.2003.12.008, 2004.
- Kalnay, E., Kanamitsu, M., Kistler, R., Collins, W., Deaven, D., Gandin, L., Iredell, M., Saha, S., White, G., Woollen, J., Zhu, Y., Leetmaa, A., Reynolds, R., Chelliah, M., Ebisuzaki, W., Higgins, W., Janowiak, J., Mo, K. C., Ropelewski, C., Wang, J., Jenne, R., and Joseph, D.: The NCEP/NCAR 40-year reanalysis project, *B. Am. Meteorol. Soc.*, 77, 737–471, doi:10.1175/1520-0477(1996)077%3C0437:TNYRP%3E2.0.CO;2, 1996.
- Kawasaki, M., Yoshioka, H., Jones, N. B., Macatangay, R., Griffith, D. W. T., Kawakami, S., Ohyama, H., Tanaka, T., Morino, I., Uchino, O., and Ibuki, T.: Usability of optical spectrum analyzer in measuring atmospheric CO<sub>2</sub> and CH<sub>4</sub> column densities: inspection with FTS and aircraft profiles in situ, *Atmos. Meas. Tech.*, 5, 2593–2600, doi:10.5194/amt-5-2593-2012, 2012.

- Keppel-Aleks, G., Toon, G. C., Wennberg, P. O., and Deutscher, N. M.: Reducing the impact of source brightness fluctuations on spectra obtained by Fourier-transform spectrometry, *Appl. Optics*, 46, 4774–4779, doi:10.1364/AO.46.004774, 2007a.
- Keppel-Aleks, G., Toon, G. C., Wennberg, P. O., and Deutscher, N. M.: Reducing the impact of source brightness fluctuations on spectra obtained by Fourier-transform spectrometry, *Appl. Optics*, 46, 4774–4779, doi:10.1364/AO.46.004774, 2007b.
- Kobayashi, N., Inoue, G., Kawasaki, M., Yoshioka, H., Minomura, M., Murata, I., Nagahama, T., Matsumi, Y., Tanaka, T., Morino, I., and Ibuki, T.: Remotely operable compact instruments for measuring atmospheric CO<sub>2</sub> and CH<sub>4</sub> column densities at surface monitoring sites, *Atmos. Meas. Tech.*, 3, 1103–1112, doi:10.5194/amt-3-1103-2010, 2010.
- König-Langlo, G.: Radiosonde During POLARSTERN Cruise PS83 (ANT-XXIX/10), Bremerhaven, Germany, doi:10.1594/PANGAEA.832783, 2014.
- Krings, T., Gerilowski, K., Buchwitz, M., Reuter, M., Tretner, A., Erzinger, J., Heinze, D., Pflüger, U., Burrows, J. P., and Bovensmann, H.: MAMAP – a new spectrometer system for column-averaged methane and carbon dioxide observations from aircraft: retrieval algorithm and first inversions for point source emission rates, *Atmos. Meas. Tech.*, 4, 1735–1758, doi:10.5194/amt-4-1735-2011, 2011.
- Lamouroux, J., Tran, H., Laraia, A., Gamache, R., Rothman, L., Gordon, I., and Hartmann, J.-M.: Updated database plus software for line-mixing in CO<sub>2</sub> infrared spectra and their test using laboratory spectra in the 1.5–2.3 μm region, *J. Quant. Spectrosc. Ra.*, 111, 2321–2331, doi:10.1016/j.jqsrt.2010.03.006, XVIth Symposium on High Resolution Molecular Spectroscopy (HighRes-2009) XVIth Symposium on High Resolution Molecular Spectroscopy, 2010.
- Masarie, K. A., Peters, W., Jacobson, A. R., and Tans, P. P.: ObsPack: a framework for the preparation, delivery, and attribution of atmospheric greenhouse gas measurements, *Earth Syst. Sci. Data*, 6, 375–384, doi:10.5194/essd-6-375-2014, 2014.
- [Boussetta, S. and Balsamo, G. and Beljaars, A. and Panareda, A.A. and Calvet, J.C. and Jacobs, C. and van den Hurk, B. and Viterbo, P. and Lafont, S. and Dutra, E. and Jarlan, L. and Balzarolo, M. and Papale, D. and van der Werf, G.: Natural land carbon dioxide exchanges in the ECMWF integrated forecasting system: Implementation and offline validation, \*Journal of Geophysical Research: Atmospheres\*, 118, No. 12, 2169–8996, doi:10.1002/jgrd.50488, 2013.](#)
- Massart, S., Agusti-Panareda, A., Aben, I., Butz, A., Chevallier, F., Crevoisier, C., Engelen, R., Frankenberg, C., and Hasekamp, O.: Assimilation of atmospheric methane products into the

- MACC-II system: from SCIAMACHY to TANSO and IASI, *Atmos. Chem. Phys.*, 14, 6139–6158, doi:10.5194/acp-14-6139-2014, 2014.
- Meirink, J. F., Eskes, H. J., and Goede, A. P. H.: Sensitivity analysis of methane emissions derived from SCIAMACHY observations through inverse modelling, *Atmos. Chem. Phys.*, 6, 1275–1292, doi:10.5194/acp-6-1275-2006, 2006.
- Messerschmidt, J., Machatangay, R., Notholt, J., Petri, C., Warneke, T., and Weinzierl, C.: Side by side measurements of CO<sub>2</sub> by ground-based Fourier transform spectrometry (FTS), *Tellus B*, 62, 749–758, doi:10.1111/j.1600-0889.2010.00491.x, 2010.
- Notholt, J., Beninga, I., and Schrems, O.: Shipborne FT-IR Measurements of Atmospheric Trace Gases on a South (33° S) to North (53° N) Atlantic Traverse, *Appl. Spectrosc.*, 49, 1525–1527, 1995.
- O'Dell, C. W., Connor, B., Bösch, H., O'Brien, D., Frankenberg, C., Castano, R., Christi, M., Eldering, D., Fisher, B., Gunson, M., McDuffie, J., Miller, C. E., Natraj, V., Oyafuso, F., Polonsky, I., Smyth, M., Taylor, T., Toon, G. C., Wennberg, P. O., and Wunch, D.: The ACOS CO<sub>2</sub> retrieval algorithm – Part 1: Description and validation against synthetic observations, *Atmos. Meas. Tech.*, 5, 99–121, doi:10.5194/amt-5-99-2012, 2012.
- PANGEA: XCO<sub>2</sub> and XCH<sub>4</sub> Total Column Measurement ANT XXIX/10 North–South Gradient, PANGEA, Bremerhaven, Germany, doi:10.1594/PANGAEA.843880, 2014.
- Peters, W., Jacobson, A. R., Sweeney, C., Andrews, A. E., Conway, T. J., Masarie, K., Miller, J. B., Bruhwiler, L. M. P., Pétron, G., Hirsch, A. I., Worthy, D. E. J., van der Werf, G. R., Rander-son, J. T., Wennberg, P. O., Krol, M. C., and Tans, P. P.: An atmospheric perspective on North American carbon dioxide exchange: CarbonTracker, *P. Natl. Acad. Sci. USA*, 104, 18925–18930, doi:10.1073/pnas.0708986104, 2007.
- Petri, C., Warneke, T., Jones, N., Ridder, T., Messerschmidt, J., Weinzierl, T., Geibel, M., and Notholt, J.: Remote sensing of CO<sub>2</sub> and CH<sub>4</sub> using solar absorption spectrometry with a low resolution spectrometer, *Atmos. Meas. Tech.*, 5, 1627–1635, doi:10.5194/amt-5-1627-2012, 2012.
- Peylin, P., Law, R. M., Gurney, K. R., Chevallier, F., Jacobson, A. R., Maki, T., Niwa, Y., Patra, P. K., Peters, W., Rayner, P. J., Rödenbeck, C., van der Laan-Luijkx, I. T., and Zhang, X.: Global atmospheric carbon budget: results from an ensemble of atmospheric CO<sub>2</sub> inversions, *Biogeosciences*, 10, 6699–6720, doi:10.5194/bg-10-6699-2013, 2013.
- [Rodgers, C. D. and Connor, B. J.: Intercomparison of remote sounding instruments, \*Journal of Geophysical Research: Atmospheres\*, 108, D3, 2156–2202, doi:10.1029/2002JD002299, 2003.](#)

- Rayner, P. J. and O'Brien, D. M.: The utility of remotely sensed CO<sub>2</sub> concentration data in surface source inversions, *Geophys. Res. Lett.*, 28, 175–178, doi:10.1029/2000GL011912, 2001.
- Rothman, L., Gordon, I., Barbe, A., Benner, D., Bernath, P., Birk, M., Boudon, V., Brown, L., Campargue, A., Champion, J.-P., Chance, K., Coudert, L., Dana, V., Devi, V., Fally, S., Flaud, J.-M., Gamache, R., Goldman, A., Jacquemart, D., Kleiner, I., Lacome, N., Lafferty, W., Mandin, J.-Y., Massie, S., Mikhailenko, S., Miller, C., Moazzen-Ahmadi, N., Naumenko, O., Nikitin, A., Orphal, J., Perevalov, V., Perrin, A., Predoi-Cross, A., Rinsland, C., Rotger, M., Šimečková, M., Smith, M., Sung, K., Tashkun, S., Tennyson, J., Toth, R., Vandaele, A., and Auwera, J. V.: The HITRAN 2008 molecular spectroscopic database, *J. Quant. Spectrosc. Ra.*, 110, 533–572, doi:10.1016/j.jqsrt.2009.02.013, 2009.
- Schepers, D., Guerlet, S., Butz, A., Landgraf, J., Frankenberg, C., Hasekamp, O., Blavier, J.-F., Deutscher, N. M., Griffith, D. W. T., Hase, F., Kyro, E., Morino, I., Sherlock, V., Sussmann, R., and Aben, I.: Methane retrievals from Greenhouse Gases Observing Satellite (GOSAT) shortwave infrared measurements: performance comparison of proxy and physics retrieval algorithms, *J. Geophys. Res.-Atmos.*, 117, D10307, doi:10.1029/2012JD017549, 2012.
- Schneider, M., Cuevas, E., Hernández, E. S., Hase, F., Blumenstock, T., García, J. C. G., and Ángel J. Gómez Peláez: Total Carbon Column Observing Network (TCCON) activities at Izaña, Tenerife, *Optica pura y aplicada*, 1–4, available at: <http://dialnet.unirioja.es/servlet/articulo?codigo=3867004> (last access: 17 July 2015), 2012.
- Schoeberl, M. R., Newman, P. A., and Lait, L. R.: Gridded meteorological data (analysis) from NMC:GG1X1:E01:SSIAVN, available at: [http://acdb-ext.gsfc.nasa.gov/Data\\_services/automaile/](http://acdb-ext.gsfc.nasa.gov/Data_services/automaile/) (last access: 17 July 2015), 2014.
- Stocker, T. F., Dahe, Q., and Plattner, G.-K.: *Climate Change 2013: The Physical Science Basis, Working Group I Contribution to the Fifth Assessment Report of the Intergovernmental Panel on Climate Change, Summary for Policymakers (IPCC, 2013)*, Cambridge University Press, Cambridge, UK and New York, NY, USA, 2013.
- TCCON-Wiki: TCCON-Wiki, available at: <https://tcon-wiki.caltech.edu/> (last access: 17 July 2015), 2015.
- Warneke, T., de Beek, R., Buchwitz, M., Notholt, J., Schulz, A., Velasco, V., and Schrems, O.: Shipborne solar absorption measurements of CO<sub>2</sub>, CH<sub>4</sub>, N<sub>2</sub>O and CO and comparison with SCIAMACHY WFM-DOAS retrievals, *Atmos. Chem. Phys.*, 5, 2029–2034, doi:10.5194/acp-5-2029-2005, 2005.

- Wunch, D., Toon, G. C., Wennberg, P. O., Wofsy, S. C., Stephens, B. B., Fischer, M. L., Uchino, O., Abshire, J. B., Bernath, P., Biraud, S. C., Blavier, J.-F. L., Boone, C., Bowman, K. P., Browell, E. V., Campos, T., Connor, B. J., Daube, B. C., Deutscher, N. M., Diao, M., Elkins, J. W., Gerbig, C., Gottlieb, E., Griffith, D. W. T., Hurst, D. F., Jiménez, R., Keppel-Aleks, G., Kort, E. A., Macatangay, R., Machida, T., Matsueda, H., Moore, F., Morino, I., Park, S., Robinson, J., Roehl, C. M., Sawa, Y., Sherlock, V., Sweeney, C., Tanaka, T., and Zondlo, M. A.: Calibration of the Total Carbon Column Observing Network using aircraft profile data, *Atmos. Meas. Tech.*, 3, 1351–1362, doi:10.5194/amt-3-1351-2010, 2010.
- Wunch, D., Toon, G., Blavier, J., Waschenfelder, R., Notholt, J., Connor, B., Griffith, D., and Sherlock-Sherlock, V.: The Total Carbon Column Observing Network, *Philos. T. Roy. Soc. A*, 369, 2087–2112, 2011, doi:10.1098/rsta.2010.0240, 2011.

**Table 1.** Leading contributions to the duration of fine-tracking control cycles of the solar tracker (average values retrieved from housekeeping data logged during the measurement campaign aboard RV *Polarstern*).

Task	Duration ms
Image acquisition	$\approx 10$
Image processing	$< 3$
Motor position request	5–10
Update motor speed	5–10
Overall average	$\approx 22$

**Table 2.** List of key retrieval parameters. The line lists are altered from the original HITRAN line lists where “mod” indicates a modification suggested by Lamouroux et al. (2010) to take line mixing effects into account. Likewise “TCCON” indicates a modification suggested by Wunch et al. (2011).

	CO <sub>2</sub>	CH <sub>4</sub>	O <sub>2</sub>	H <sub>2</sub> O
spectral window cm <sup>-1</sup>	6173–6390	5897–6145	7765–8005	8353.4–8463.1
line list	HITRAN08 (mod)	HITRAN08	HITRAN08 (TCCON)	HITRAN09 (TCCON)
disturbing gas	H <sub>2</sub> O, CH <sub>4</sub>	H <sub>2</sub> O, CO <sub>2</sub>	H <sub>2</sub> O	–
continuum points	40	20	25	5
sza dependency ( $\Theta = 80^\circ$ )	≈ 0.6 %	≈ 0.4 %	none	not assessed
<a href="#">a priori profile</a>	<a href="#">CAMS</a>	<a href="#">CAMS</a>	<a href="#">static</a>	<a href="#">CAMS</a>

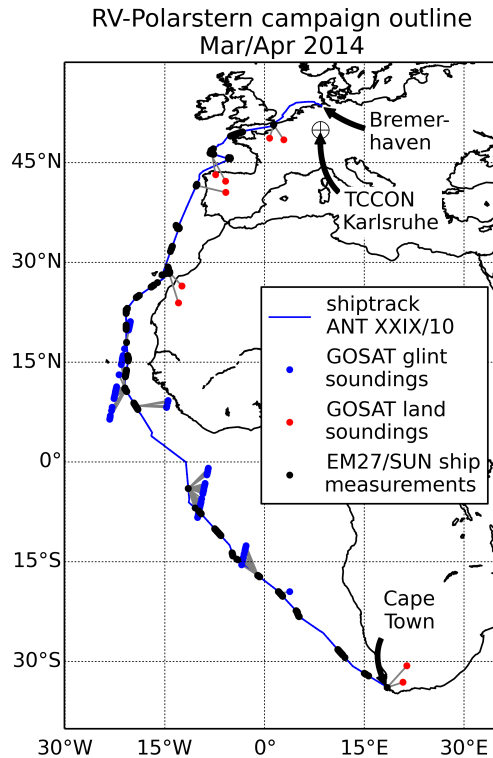


**Figure 1.** The ship track of the ANT XXIX/10 RV *Polarstern* cruise (blue line). Valid data is marked black. GOSAT-soundings that coincide with ship based measurements within  $\pm 4$  h and  $5^\circ$  (lat, lon) are marked in blue (ocean) and red (land) and interconnected (gray lines).

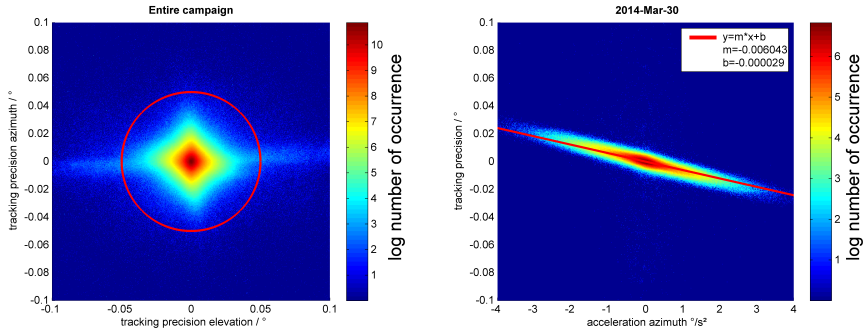


**Figure 2.** Both figures show occurrence of tracking errors in logarithmic color code. The left figure counts azimuth and elevation tracking errors for the entire campaign record. The red circle defines the desired  $0.05^\circ$  tracking precision. 98.7% of the data points are within the circle. The right figure shows azimuth tracking precision vs. angular azimuthal acceleration for a representative day with significant angular accelerations due to a rougher sea than other days.

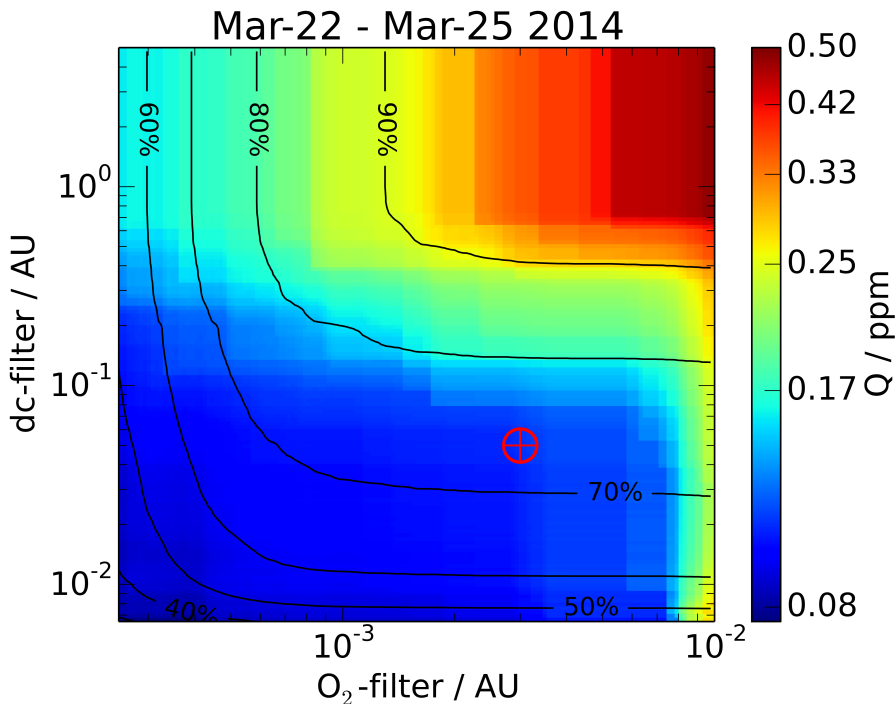


**Figure 3.** Effect of filter threshold for the O<sub>2</sub>-filter (abscissa) and the DC-filter (ordinate) on the standard deviation of retrieved XCO<sub>2</sub> (color coded in logarithmic scale). Standard deviation of XCO<sub>2</sub> is calculated for four sample days after subtracting a 3rd order polynomial that accounts for diurnal and day-to-day variability. The data yield is overlaid as solid black contours. The finally chosen filter thresholds (5 % for the DC-filter and 0.3 % for the O<sub>2</sub>-filter) are marked with the red marker.

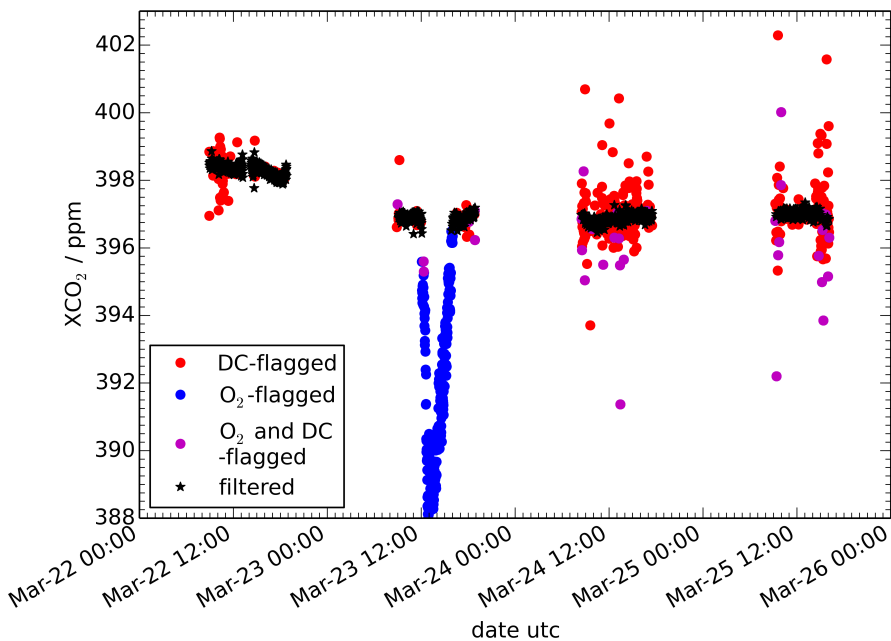


**Figure 4.** Effect of the DC-filter and the O<sub>2</sub>-filter on the retrieved XCO<sub>2</sub> for four sample days during the campaign. The outlier on 23 March that is caught by the O<sub>2</sub>-filter originates from a malfunction of the sun-tracker that caused instable unstable pointing. The days after were affected by small but opaque clouds that disturbed some measurements which is caught by the DC-filter.

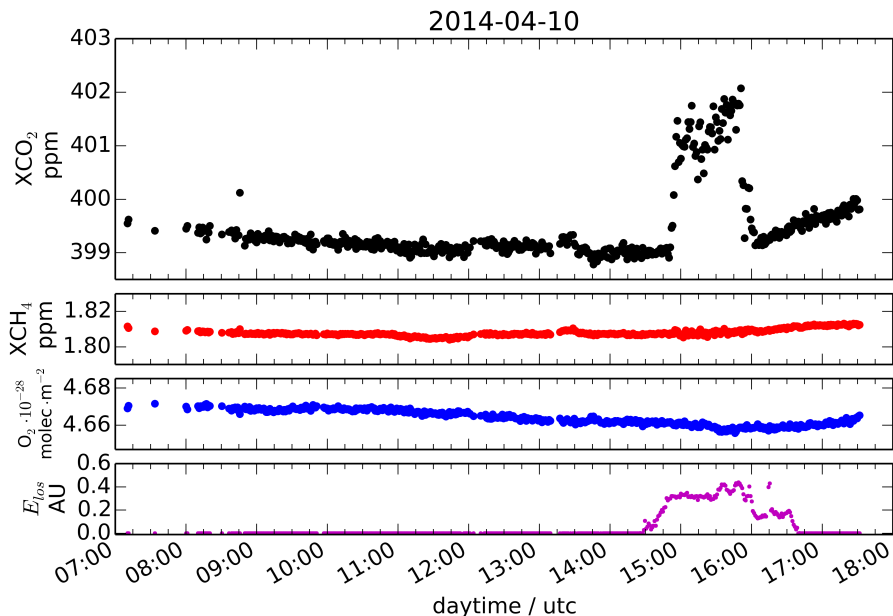


**Figure 5.** XCO<sub>2</sub> (top) record for a representative day after applying the DC and O<sub>2</sub> quality filters. The XCH<sub>4</sub> (upper middle, red) and O<sub>2</sub> (lower middle, blue) retrievals indicate no enhancements. In contrast, the XCO<sub>2</sub> enhancement of more than 2 ppm between 3–5 p.m. can be related to the lines-of-sight crossing the ship's exhaust plume. The calculated enhancement  $E_{\text{los}}$  (bottom) drives the EP-filter with a rejection threshold set at 0.001.

~~Daily averages of the modulation efficiency driving the adopted ILS retrieved from absorption lines during the campaign. A sudden step of 1 can be observed after the instrument housing was opened on 18 March 2014.~~

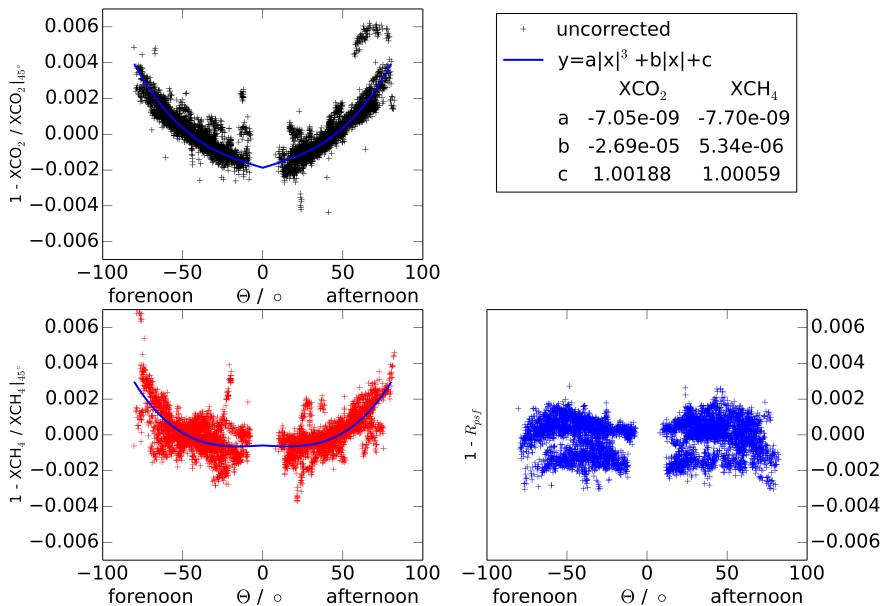


**Figure 6.** SZA dependency for CO<sub>2</sub> (upper left, referenced to XCO<sub>2</sub> at forenoon/afternoon SZA = 45°), CH<sub>4</sub> (lower left, referenced to XCH<sub>4</sub> at forenoon/afternoon SZA = 45°), and O<sub>2</sub> (lower right, surface pressure referenced O<sub>2</sub> retrieval  $R_{\text{psf}}$  [see](#) Eq. (3)) as a function of SZA  $\theta$ . Solid lines show the fitted SZA correction function.

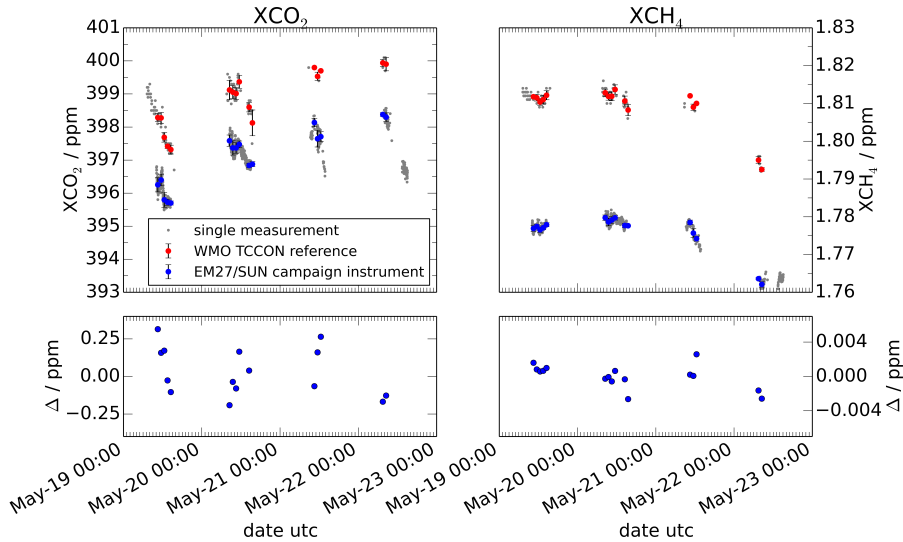


**Figure 7.** Post campaign measurements in Karlsruhe are used to retrieve the WMO-calibration factor for each gas. Hourly averages are taken for the TCCON reference (red) and the EM27/SUN measurements (blue). The calibration residual (lower panel) is defined as  $\Delta := \langle X_{\text{wmo}} \rangle_h - \langle X_{\text{gas,wmo}} \rangle_h$ .

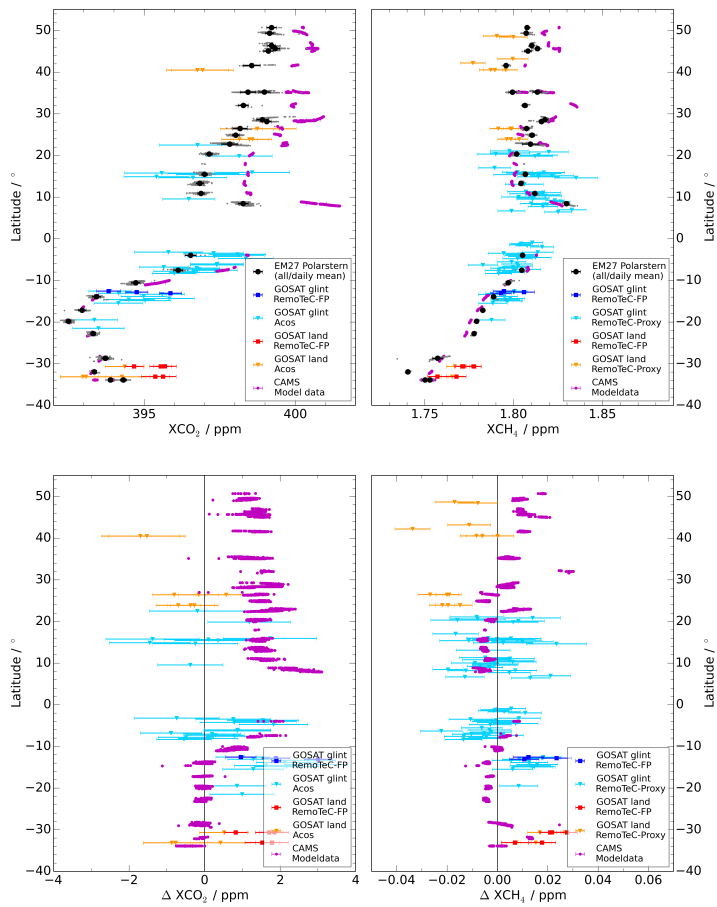


**Figure 8.** Latitudinal transects of  $XCO_2$  (left) and  $XCH_4$  (right) for the ship-borne EM27/SUN measurements (daily averages black dots, all data gray dots) and various correlative data sets (top) as well as differences of the latter to our ship records (bottom). For  $XCO_2$ , correlative datasets are the RemoTeC-FP retrievals from GOSAT (ocean-glint blue, land-nadir red), the ACOS retrievals from GOSAT (ocean-glint light blue, land-nadir orange), and  $XCO_2$  modeled by the [MAGG-II-CAMS](#) model (purple). For  $XCH_4$ , correlative datasets are the RemoTeC-FP retrievals from GOSAT (ocean-glint blue, land-nadir red), the RemoTeC-Proxy retrievals from GOSAT (ocean-glint light blue, land-nadir orange), and  $XCH_4$  modeled by the [MAGG-II-CAMS](#) model (purple). For GOSAT, soundings are coincident whenever they are conducted within  $5^\circ$  latitude/longitude of the ship track and within a  $\pm 4$ h time frame.  $XCO_2$  and  $XCH_4$  differences shown in the lower panels are calculated according to  $\Delta = X - \langle X_{EM27} \rangle_{4h}$  where the brackets indicate averaging over 4 h.

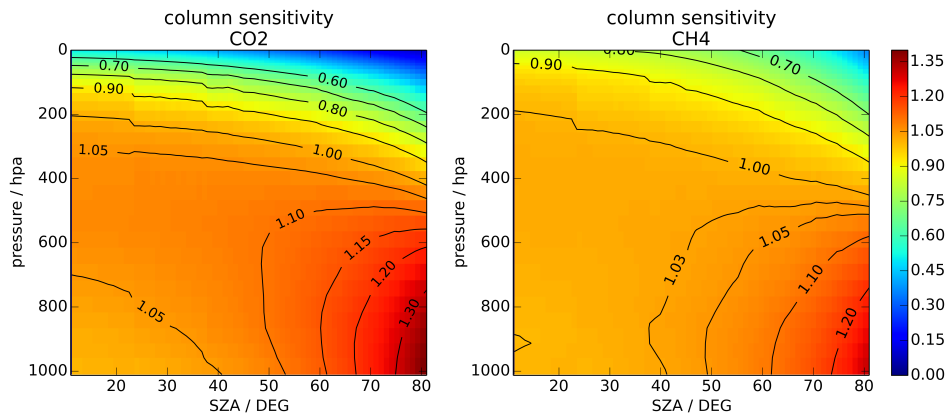


**Figure 9.** Retrieval total column sensitivity of the target species in dependence of the layer pressure and solar zenith angle (SZA). The data is averaged over three consecutive campaign days (Mar 24th, Mar 31th and Apr. 8th). The figures can be interpreted as the factor that the total column product will be enhanced, if one additional molecule would be added to a distinct pressure layer.